Measurement: Food 19 (2025) 100241

Contents lists available at ScienceDirect

Measurement: Food

journal homepage: www.elsevier.com/locate/meafoo

Authentication of avocado oil mixed with cooking oils (branded and loose palm oil) utilizing fourier transform infrared spectroscopy in conjunction with chemometrics

David Fernando [a,b,c], Desy Ayu Irma Permatasari [b], Agustina Ari Murti Budi Hastuti [b,c], Abdul Rohman [b,c,*]

[a] Master in Pharmaceutical Sciences, Faculty of Pharmacy, Universitas Gadjah Mada, Jl. Sekip Utara, Sleman, Yogyakarta 55281, Indonesia
[b] Department of Pharmaceutical Chemistry, Faculty of Pharmacy, Universitas Gadjah Mada, Yogyakarta, Indonesia
[c] Centre of Excellence, Institute of Halal Industry and Systems, Universitas Gadjah Mada, Yogyakarta, Indonesia

ARTICLE INFO

Keywords:
Adulteration
Authentication
Safety
Quality
Edible oils

ABSTRACT

Avocado oil (AVO) has become popular for its health advantages and culinary variety, while its elevated cost has rendered it susceptible to adulteration practices, frequently with less expensive edible oils such as palm oil. Attenuated total reflectance-fourier transform infrared spectroscopy (ATR-FTIR) in conjunction with chemometrics is a promising way to quickly, rapidly, and non-destructively detect AVO adulterated with branded palm oil (BPO) or loose palm oil (LPO). AVO can be distinctly categorized apart from BPO and LPO using FTIR analysis corroborated by principal component analysis (PCA). Principal component (PC) 1 is primarily influenced by absorption at a wavenumber of 1743 cm^{-1}, whereas PC2 is impacted by absorption at a wavenumber of 2953 cm^{-1}. With first derivative data and multiplicative scatter correction (MSC), multivariate calibration of principal component regression (PCR) was able to correctly predict the amount of BPO in AVO. This approach yielded root mean squared error of calibration (RMSEC) and root mean square error for prediction (RMSEP) values of 0.56 and 0.55, alongside coefficient of determination for the calibration and prediction model (R^2-cal and R^2-val) values of 0.9998 and 0.9999, respectively. In addition, PCR using first-derived data without MSC adjustment accurately quantified BPO levels in AVO, with RMSEC and RMSEP values of 0.60 and 0.61, respectively, along with R^2-cal and R^2-val values of 0.9998. This PCA-based discriminant analysis correctly separated the real AVO samples from the adulterated AVO samples with classification accuracies of 98.18 % for BPO and 100 % for LPO. This method may also be applicable further for detecting other possible edible oil adulteration, including soybean oil, rapeseed oil, and sunflower oil.

Introduction

AVO has recently experienced a notable increase in popularity [1]. This rise is attributed to its utility across various industries, owing to its elevated concentrations of monounsaturated fatty acids (MUFA) similar to olive oil and its neutral flavor profile [2,3]. AVO has been acknowledged for its health benefits, including the prevention of cardiovascular diseases by reducing low-density lipoprotein absorption and exhibiting anti-inflammatory qualities [4]. According to a review by Lin and Li [5], AVO is advantageous not only for cardiovascular illnesses but also for addressing diabetes, inflammation, oxidative stress, and obesity [5]. Consequently, AVO remains a focal point for the food, pharmaceutical, and cosmetic industries, while also garnering heightened interest in fields such as structured lipids, nanotechnology, and environmental stewardship [6].

Pérez-Calabuig et al. [1] reported that AVO price exceeds that of other oils, ranging from 10 to 15 € per 250 mL. The elevated demand and popularity of this health-promoting material, along with the substantial expense of the fruit and the expensive methods required to increase yield (such as centrifugation, aqueous separation, pressure techniques, or solvent extraction), exacerbate the situation. Palm oil, for example, priced at approximately 923.91 USD per metric ton or 0.9 USD per

* Corresponding author at: Department of Pharmaceutical Chemistry, Faculty of Pharmacy, Universitas Gadjah Mada, Jl. Sekip Utara, Sleman, Yogyakarta 55281, Indonesia.
E-mail address: abdul_kimfar@ugm.ac.id (A. Rohman).

https://doi.org/10.1016/j.meafoo.2025.100241
Received 15 April 2025; Received in revised form 28 June 2025; Accepted 8 July 2025
Available online 9 July 2025
2772-2759/© 2025 The Authors. Published by Elsevier Ltd. This is an open access article under the CC BY license (http://creativecommons.org/licenses/by/4.0/).

kilogram [7], is significantly less expensive than AVO. This example elucidates the reasons for the product's susceptibility to diverse unlawful adulterations [1]. Furthermore, a bibliometric study conducted by Fernando et al. [8] indicated that keywords related to AVO adulteration have gained prominence in the past decade relative to prior studies, implying an increased scholarly interest in the topic of AVO adulteration.

Food fraud can occur intentionally or unintentionally, such as by adulteration, which involves the incorporation of a component that compromises the original quality and purity of the food for economic gain. The primary forms of adulteration include substitutions, dilutions, and the disguise of processes and/or components [9,1]. Since these procedures typically lack ethical labeling, they may lead to significant health problems, risks of foodborne illness epidemics, or even fatalities due to food intake [10,11]. Numerous initiatives have been made to address these challenges, including food safety rules (such as standards of identification and EU geographical indicator schemes), hazard analysis, food fraud vulnerability assessments, and analytical detection. Analytical detection strategies, in particular, are a crucial element of a food fraud prevention program and can verify the accuracy of ingredient claims in pertinent documents [12].

Conventional techniques for detecting adulteration include polymerase chain reaction, chromatography, and immunological approaches, which are extensively documented and commonly employed to verify authenticity and identify adulteration [13]. Despite displaying a high degree of consistency, these approaches are time-consuming, labor-intensive, and require highly skilled individuals. Consequently, they are inefficient for real-time and high-throughput routine analysis. No one screening approach presently identifies all adulterants; hence, it is prudent to employ numerous non-targeted techniques, like near-infrared spectroscopy, liquid chromatography coupled with two-dimensional mass spectrometry, or nuclear magnetic resonance. The efficacy of these procedures is contingent upon the quality and representativeness of reference samples [12]. Among the discussed methods, FTIR spectroscopy is characterized as cost-efficient in several review studies related to analytical detection aimed at combating food fraud practices [14,15].

FTIR spectroscopy, combined with chemometric modeling, has effectively distinguished authentic AVO in binary mixtures with soybean oil, grapeseed oil [16], sunflower oil, and canola oil [17], as well as in ternary mixtures with sunflower and soybean oil [18]. No research, however, has been conducted to verify the authenticity of AVO in comparison to less expensive oils, such as BPO or LPO, despite its potential as a cost-effective adulterant. Therefore, this research aims to employ FTIR spectroscopy fingerprinting in conjunction with chemometric techniques as a speedy, cost-efficient, non-destructive, and versatile method to address adulterations in AVO, particularly against inexpensive and widely available cooking oils such as BPO and LPO. This research contributes to method development and offers practical approaches for verifying the authenticity and safety of AVO, potentially impacting food safety standards and regulations.

Materials and methods

Sample acquisition

Avocado specimens are gathered from ten distinct locations/varieties, yielding a total of ten samples (Table 1). The authenticity of avocados was obtained in the Department of Pharmaceutical Biology under supervision by Prof. Dr. Erna Prawita, Faculty of Pharmacy, Gadjah Mada University, Indonesia. The collected samples are allowed to mature (at room temperature) before being converted into dried avocados using the conventional oven. The chosen avocados will undergo pre-processing, which entails washing, peeling, seed separation, and pulp slicing. The avocado utilized in this investigation is a ripe specimen appropriate for consumption. The avocado's flesh is detached from the seeds and the peel, and only the mesocarp is used throughout the oil extraction process. The avocado pulp is diced into small pieces and spread thinly (about 1 cm) on an aluminium foil foundation for drying. Drying is conducted in a dryer oven at a consistent temperature of 50 °C for approximately 24 h.

The extraction procedure refers to the study by Santana et al. [19], with some modifications. Briefly, one hundred grams of dried avocados were extracted using n-hexane solvents at a 1:3 wt/wt ratio. Extraction is conducted for one hour utilizing sonication at a temperature of 45 °C. The temperature is regulated through the application of ice cubes to ensure that the extraction temperature remains within $45\ ^{\circ}C \pm 5\ ^{\circ}C$. The extracted sample undergoes filtration with filter paper, followed by the evaporation of n-hexane. The evaporation method refers to the research of Nasri et al. [20], using a rotary evaporator. The rotary evaporator is configured to a rotation speed of 100 rpm at 50 °C. Solvent reduction is conducted until the solvent ceases to drip. AVO is subsequently chilled in an ice bath for 10 min and then re-dissolved (winterization). The solution is subsequently filtered using Whatman No 1 paper. The filtration process is repeated using a rotating evaporator set at a speed of 100 rpm and a temperature of 50 °C, and the whole process is replicated thrice. AVO samples are preserved in a refrigerator in a dark bottle until the assessment is conducted.

Ten BPO samples were purchased from supermarkets in Yogyakarta, Indonesia. All of them were analyzed within the best-before date, and from the time of acquisition until the measurements were performed, they were maintained in a dry and dark cabinet. Specifically, retail palm oils from the brands Fortune, Bimoli, Sania, Tawon, Rizki, Hemart, Tropical, Rose Brand, Fitri, and Sunco were used in the study. Meanwhile, the LPOs were collected from the several grocery stores in the traditional market at Yogyakarta, consisting of sizes 0.5 and 1.0 kg with primary packaging made of plastics tied with rubber bands. The product specifications, such as claims, primary packaging type, manufacturer (country), packing volume, expiration date, and product price, are shown in Table 2 (BPO) and Table 3 (LPO).

Table 1
Collection of Ten Avocado Samples from Different Regions.

Sample	Date	Region	Province	Coordinate	Soil Type	Variety	Height (m asl)
AVO1	16/03/2024	Tawangmangu	Central Java	7°40′13″S 111°7′2″E	Andosol	Mentega	994
AVO2	23/05/2024	Magetan	East Java	7°44′30″S 111°14′20″E	Sandy	Mentega	835
AVO3	28/05/2024	Karangpandan	Central Java	7°37′41″S 111°5′20″E	Volcanic	Local	726
AVO4	15/07/2024	Tawangmangu	Central Java	7°39′51″S 111°7′26″E	Volcanic	Mentega	1.019
AVO5	1/09/2024	Tawangmangu	Central Java	7°40′11″S 111°7′28″E	Volcanic	Wulung	1.030
AVO6	21/09/2024	Semarang	Central Java	7°14′19″S 110°23′22″E	Rice husk + manure	Pangeran	663
AVO7	21/09/2024	Blitar	East Java	8°8′16″S, 112°9′46″E	Clay soil + manure	Alligator/ Florida	156
AVO8	23/09/2024	Bandar Lampung	Lampung	5°20′14″S 105°12′55″E	Red laterite	Mentega	118
AVO9	27/10/2024	Semarang	Central Java	7°14′19″S 110°23′22″E	Rice husk + manure	Kendil	663
AVO10	27/10/2024	Semarang	Central Java	7°14′19″S 110°23′22″E	Rice husk + manure	Wina	663

Table 2
List of Branded Palm Used.

Sample label	Brand	Product Composition	Primary Packaging	Volume (mL)	Price (USD)*	Price (USD)/L*
BPO1	Fortune	Palm oil + Vitamin A	Clear Plastic Packs	800	0.97	1.21
BPO2	Bimoli	Palm oil + Vitamin A	Clear Plastic Packs	1000	1.34	1.34
BPO3	Sania	Palm oil + Vitamin A	Clear Plastic Packs	800	0.97	1.21
BPO4	Tawon	Palm oil + Vitamin A	Clear Plastic Packs	900	1.04	1.15
BPO5	Rizki	Palm oil + Vitamin A	Clear Plastic Bottles	800	0.95	1.19
BPO6	Hemart	Palm oil + Vitamin A	Clear Plastic Bottles	500	0.61	1.22
BPO7	Tropical	Palm oil + Vitamin A	Clear Plastic Bottles	1000	1.21	1.21
BPO8	Rose Brand	Palm oil + Vitamin A	Clear Plastic Cups	220	0.25	1.14
BPO9	Fitri	Palm oil + Vitamin A	Clear Plastic Bottles	200	0.26	1.30
BPO10	Sunco	Palm oil + Vitamin A	Clear Plastic Packs	1000	1.35	1.35

Convert rate 1 USD = 16.33 IDR, *rounded to 2 decimal places.

Table 3
List of Loose Palm Used.

Sample label	Source	Seller's Claim	Primary Packaging	Weight (kg)	Price (USD)*	Price (USD)/kg*
LPO1	Colombo Market	Palm oil	Clear Plastic Packs	0.5	0.67	1.22
LPO2	Colombo Market	Palm oil	Clear Plastic Packs	1.0	1.07	1.07
LPO3	Kliwon Market, Berbah	Palm oil	Clear Plastic Packs	1.0	1.10	1.10
LPO4	Kliwon Market, Berbah	Palm oil	Clear Plastic Packs	0.5	0.61	1.22
LPO5	Kliwon Market, Berbah	Palm oil	Clear Plastic Packs	0.5	0.54	1.08
LPO6	Kliwon Market, Berbah	Palm oil	Clear Plastic Packs	0.5	0.62	1.24
LPO7	Kranggan Market	Palm oil	Clear Plastic Packs	0.5	0.61	1.22
LPO8	Kranggan Market	Palm oil	Clear Plastic Bottle	0.25	0.31	1.24
LPO9	Pogung Lor	Palm oil	Clear Plastic Packs	0.5	0.61	1.22
LPO10	Pogung Baru	Palm oil	Clear Plastic Packs	0.5	0.73	1.46

Convert rate 1 USD = 16.33 IDR, *rounded to 2 decimal places.

ATR-FTIR measurement and characterization of AVO against BPO and LPO

FTIR spectra of the oil samples were collected according to protocols established by Fernando et al. [21]. The spectra were obtained with a Thermo Nicolet iS10 instrument (ThermoFisher Scientific), equipped with a Deuterated Triglycine Sulfate (DTGS) detector and employing an ATR diamond crystal sampling method. The parameters were set at a resolution of 4 cm^{-1} utilizing 32 scans in the mid-infrared region (MIR) from 4000 to 600 cm^{-1}. The sample oil was applied to the ATR surface at ambient temperature (about 25 °C). A background scan was performed, and the ATR surface was sanitized with 96 % ethanol (pro analysis) before sample scanning. Prior to proceeding to the next sample, the ATR surface was cleansed with n-hexane (pro analysis) and wiped down. All specified reagents were obtained from Merck (Darmstadt, Germany). Prior to scanning each sample, an air background spectrum was recorded to minimize spectral variability and ensure measurement consistency. Background monitoring was conducted immediately before every individual sample reading. The spectra were analyzed and displayed with OMNIC® software and recorded as absorbance values.

The extracted samples of AVO were combined (replicates) and analyzed via ATR-FTIR four times, yielding four data points for each sample. Ten samples each of BPO and LPO will be analyzed using ATR-FTIR four times, yielding four data points for each sample. MetaboAnalyst software version 6.0 was used to analyze the FTIR data from AVO, BPO, and LPO samples using PCA. At this stage, we expect to group the samples according to their respective identities, specifically the AVO, BPO, or LPO groups. The same software will also visualize the correlation between the sample and the dependent variables as a heatmap. A PCA model that explains the greatest variation and visualization in both 2-dimensional and 3-dimensional terms will be discussed.

Authentication of AVO from BPO and LPO

FTIR data of samples consisting of a mixture of AVO, BPO, and LPO at concentrations of 0 %, 10 %, 20 %, 30 %, 40 %, 50 %, 60 %, 70 %, 80 %, 90 %, and 100 % were studied. Using chemometric regression through TQ Analyst™ software version 9. Five sets of experimental data will be divided into three calibration datasets and two external validation datasets. Regression analysis was conducted utilizing classical least squares (CLS), stepwise multiple linear regression (SMLR), partial least squares (PLS), and PCR methodologies, incorporating pre-processed spectral variations (MSC) and data derivatization (first and second derivatives). The optimal model was identified based on the RMSEC and R^2-cal calibration parameters, as well as the external validation parameters RMSEP and R^2-val. The RMSEP parameters should be <1.2 times the RMSEC, with R^2-cal and R^2-val parameters maximized [22]. Subsequently, a one-sample *t*-test will be conducted utilizing IBM SPSS® Statistics software version 29.0 utilizing the calculated and actual concentrations. If the actual findings and calculations do not differ significantly at the 95 % confidence level, the model is deemed successful. The model aims to quantify the percentage of adulteration of BPO or LPO in the AVO sample.

The discriminant analysis based on PCA was conducted using TQ Analyst™ software version 9 with the same dataset. The training program assesses whether the sample is classified as false using BPO, LPO, or neither. In this case, the algorithm will be instructed to categorize samples into three primary datasets: pure AVO, pure BPO or LPO, and adulterated samples. The five datasets will be divided into three sets of calibration data and two sets of external validation data. The discriminant analysis is deemed successful if a majority or all of the 55 sample readings are classified correctly.

Results and discussion

Characterization between AVO, BPO, and LPO

Spectral samples comprising AVO, BPO, and LPO are illustrated in Fig. 1, highlighting 16 distinct peaks due to the absorption of the

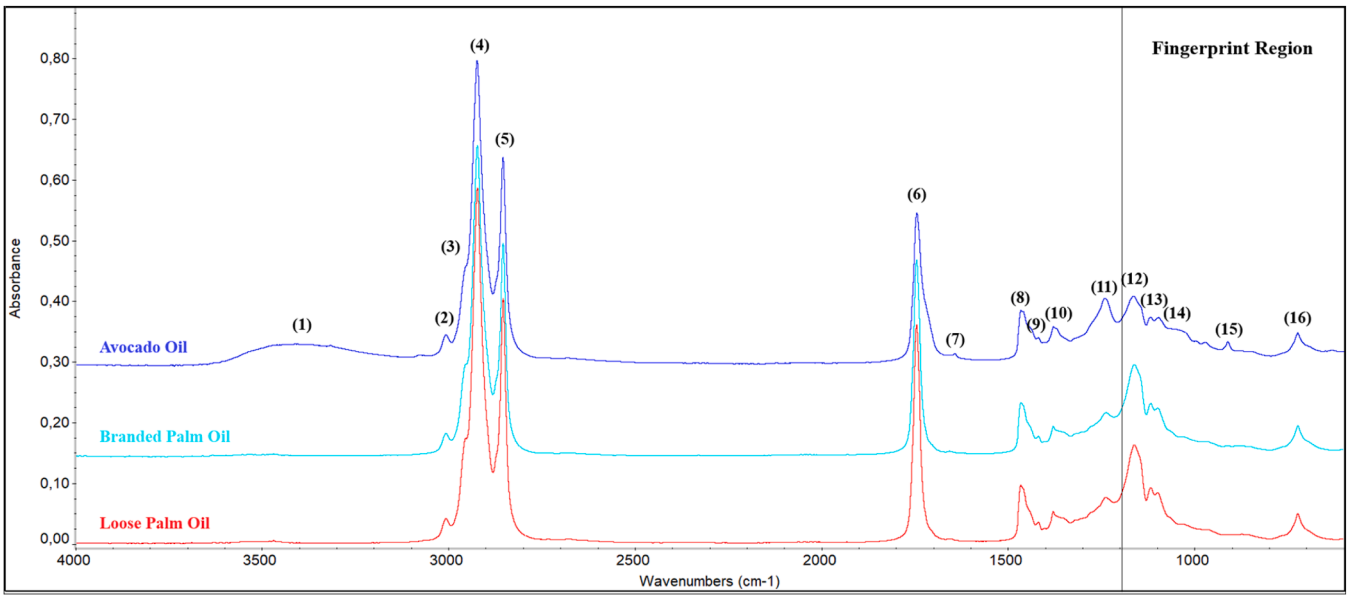


Fig. 1. Spectra Representatives of AVO, BPO, and LPO Absorption Marked with Numbers 1–16.

important functional groups present in the AVO. The peak absorptions, functional groups, vibrational modes, intensities, and wavenumbers were interpreted according to Coates (2006), Lerma-García et al. [23], as shown in Table 4. The -OH stretch observed at a wavenumber of 3428 cm^{-1} may signify the presence of free fatty acids generated during hydrolysis, together with phytosterol molecules like β-sitosterol and campesterol [24].

AVO, BPO, and LPO were acquired from ten locations and measured using FTIR four times for characterization purposes. Data from all AVO, BPO, and LPO across ten locations were analyzed using PCA, with the intensity peak represented as concentration. The 2D PCA biplot in Fig. 2A illustrates that the AVO sample is distinguishable from BPO and LPO, as evidenced by the differing group formations. BPO cannot be separated from LPO because both groups are situated in the same location. Despite the inclusion of the PC3 factor in the 3D PCA (Fig. 2B), the BPO and LPO samples did not segregate into distinct groups. Fig. 2A also illustrates that BPO has more similarity to AVO compared to LPO. BPO has a broader distribution than LPO; consequently, when analyzed using PC1 (which captures the majority of total variation), specific segments of AVO overlap with BPO, while LPO is clearly distinguishable from AVO, as there is no intersection between the two samples.

The PC1 is characterized by absorption at a wavenumber of 1743 cm^{-1}, with an eigenvector value of −0.68588; in contrast, PC2 is defined by absorption at a wavenumber of 2953 cm^{-1}, with an eigenvector value

Table 4
Interpretation Spectra Infrared Samples of AVO, BPO, and LPO [25,23,26].

No.	Wavenumber detection (cm^{-1})	Interpretation group function	Vibration mode	Intensity	Wavenumber range reference (cm^{-1})	Potential compound
1	3428	-OH	OH stretching	Broad	3200–3570	Carboxylic acid, free fatty acids, β-sitosterol, campesterol
2	3005	=CH (*cis*)	Cis =CH stretching	Weak	3029–2989	Alkenes (MUFA/ PUFA)
3	2953	-CH (CH_3)	CH stretching (asymmetric)	Strong	2989–2946	Alkane
4	2922	-CH (CH_2)	CH stretching (asymmetric)	Strong	2946–2881	Alkane
5	2853	-CH (CH_2)	CH stretching (symmetrical)	Strong	2881–2782	Alkane
6	1743	-*C* = *O* (ester)	*C* = *O* stretching	Strong	1750–1725	Esther
7	1641	-HC=CH-	Alkenyl *C* = *C* stretching	Moderate-weak	1680–1620	Alkene
8	1463	-CH (CH_2)	CH bending (scissoring)	Weak	1486–1446	Alkane
9	1418	=CH (*cis*)	Terminal =CH in-plane bend (rocking)	Weak	1420–1410	Alkenes (MUFA/PUFA)
10	1376	-CH (CH_3)	CH bending (symmetric)	Weak	1380–1370	Alkane
11	1239	-CO or -CH_2-	CO stretching or CH bending	Strong	1290–1211	Ester, ether
12	1162	-CO or -CH_2-	CO stretching or CH bending	Strong	1211–1147	Ester, ether
13	1118	-C-OH or -COC-	CO stretching	Strong	1128–1106 (alkyl substituted ether), ±1100 (secondary alcohol)	Alcohol, ether
14	1098	-C-OH or -COC-	CO stretching	Strong	1106–1072 (alkyl substituted ether), ±1100 (secondary alcohol)	Alcohol, ether
15	966	-HC=CH- (trans)	=CH bending (out of plane)	Strong	970–960	Alkenes (MUFA/PUFA)
16	721	-HC=CH- (*cis*) or -$(CH_2)_n$-	=CH bending (out of plane) or rocking	Wide	754–701	Alkane

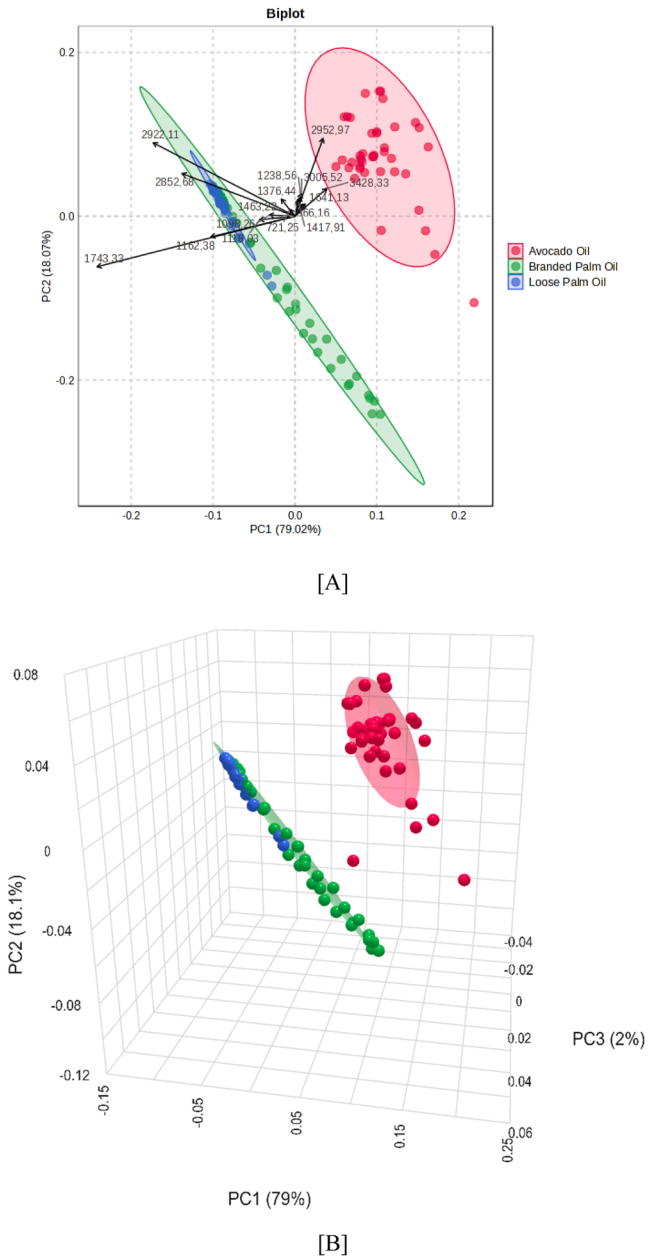


Fig. 2. 2D PCA Biplot [A] and 3D PCA Score Plot [B] of AVO, BPO, and LPO samples.

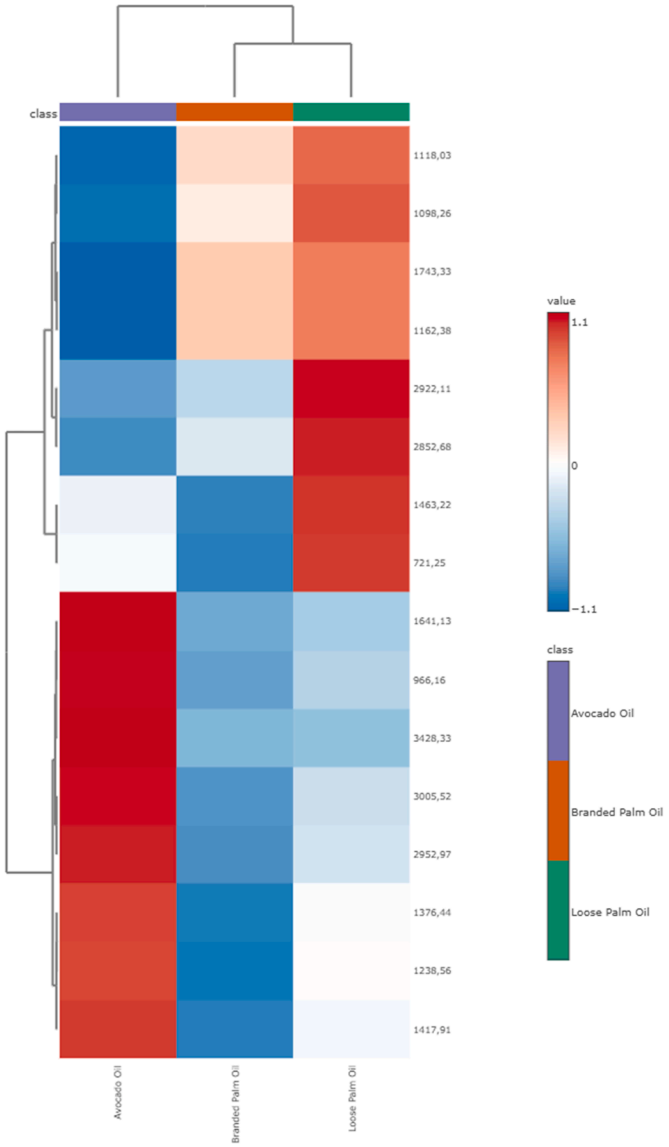


Fig. 3. Heatmap (Euclidean Distance) Visualization between AVO, BPO, and LPO.

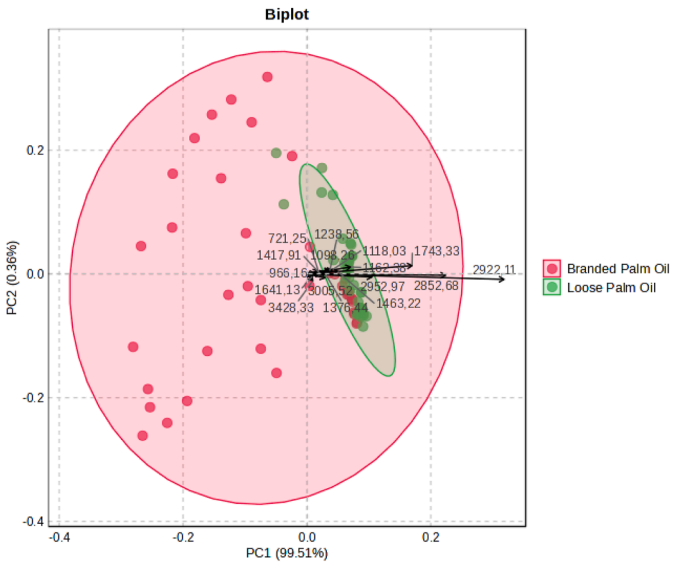
of 0.56388. PC1 (79.02 %) and PC2 (18.07 %) together represent 97.09 % of the data variation in two-dimensional PCA, whereas PC3 (2 %) increases the explained variance to 99.1 % in three-dimensional PCA. The principal determinants affecting PC3 are absorption at 2953 cm^{-1} and 1239 cm^{-1}, with associated eigenvector values of −0.623 and 0.595, respectively. The intensity absorption parameters were analyzed by a heatmap to determine the similarities among AVO, BPO, and LPO.

The hierarchical analysis of the heatmap (Fig. 3) indicates that the BPO sample demonstrates a higher degree of resemblance to LPO. This variability may be attributed to discrepancies in material specifications within oil production. The BPO and LPO samples showed relatively larger intensities at wavenumbers of 2922 cm^{-1}, 2853 cm^{-1}, 1118 cm^{-1}, 1098 cm^{-1}, 1743 cm^{-1}, and 1162 cm^{-1} compared to AVO. The AVO, on the other hand, showed a comparatively greater intensity at wavenumbers of 1641 cm^{-1}, 966 cm^{-1}, 3428 cm^{-1}, 3006 cm^{-1}, 2953 cm^{-1}, 1376 cm^{-1}, 1239 cm^{-1}, and 1418 cm^{-1}. AVO samples were excluded, and PCA was performed. The objective was to establish a more distinct classification between BPO and LPO.

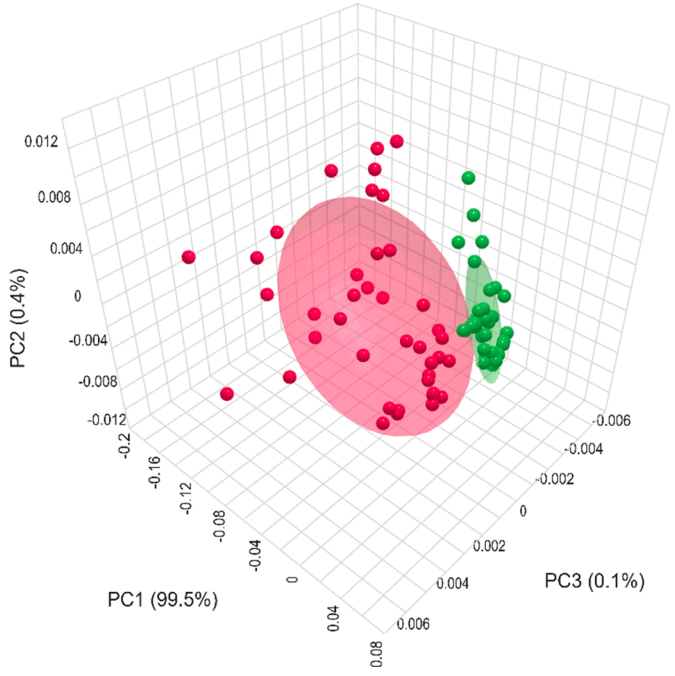
The 2D PCA biplot in Fig. 4A indicates that the BPO sample is indistinguishable from LPO, as the LPO grouping occupies the same region as BPO. With the incorporation of the PC3 factor in 3D PCA (Fig. 4B), the BPO and LPO samples started to separate into different clusters. The principal determinant for PC1 is absorption at a wavenumber of 2922 cm^{-1}, with an eigenvector value of 0.70139, while for PC2, it is absorption at a wavenumber of 1743 cm^{-1}, with an eigenvector value of 0.49542. PC1 (99.51 %) and PC2 (0.36 %) together represent 99.87 % of the variation in the 2D PCA analysis. The incorporation of PC3 (0.1 %) increases the overall explained variance to 99.97 % in 3D PCA. The principal influences on PC3 are the absorptions at 3006 cm^{-1} and 2953 cm^{-1}, with associated eigenvector values of −0.612 and −0.598, respectively.

Authentication of AVO from BPO and LPO

Multivariate modeling was conducted to determine the presence and concentration of palm oil in mixtures containing AVO, particularly given that the adulterant levels do not exceed 30 %. Thus, quantifying the palm oil content is more relevant than measuring the already



[A]



[B]

Fig. 4. 2D PCA Biplot [A] and 3D PCA Score Plot [B] of BPO and LPO Samples.

predominant AVO. Various multivariate calibrations, including CLS, SMLR, PLS, and PCR, are examined. We aim to determine the most effective model for quantifying BPO and LPO in a binary mixture using AVO. Binary mixes of spectral fingerprint finger samples are measured and analyzed via TQ Analyst™. Calibration and validation parameters for the binary mixture of AVO and BPO are presented in Table 5.

Optimal modeling for the quantification of BPO in the AVO binary mixture was obtained using PCR chemometrics with MSC pre-processing and first derivative data and included the extended wavenumbers of 1735–901 cm^{-1}. The model primarily utilizes MSC pre-processing and generated data to mitigate disturbance effects on baseline variation and enhance the quality of spectral data. This model yields the lowest RMSEC and RMSEP values, specifically 0.56 and 0.55, indicating a very low error level in the calibration and validation processes. Furthermore, the R^2-cal and R^2-val values are nearly equal to 1, namely 0.9998 and 0.9999, respectively, signifying that this model possesses a remarkably strong predictive capability and can elucidate nearly all variance in the data. The RMSEP/RMSEC value of 0.98, which is near 1, indicates a minimal likelihood of overfitting, as the calibration model yields results nearly identical to those of the validation model. This model not only possesses excellent accuracy but is also trustworthy for the quantification of BPO in a binary mixture with AVO. In addition, the PCR model without MSC pre-processing of first derivative data produces satisfactory findings utilizing absorption from wavenumbers 1163–890 cm^{-1}. The model's ability to yield high R^2-cal and R^2-val values (0.9995 and 0.9996, respectively) and low RMSEC and RMSEP values (0.95 and 0.85, respectively) in the absence of MSC indicates that the underlying signal in the first derivative FTIR spectra is sufficiently robust and informative for precise measurement.

Calculation results from the models were assessed using hypothesis testing to ascertain whether the present findings deviate significantly from the calculated values. Results of the normality test and hypothesis test are reported in Table 6. Statistical analysis The Shapiro-Wilk normality test, one-sample *t*-test, and Wilcoxon signed-rank test were conducted utilizing IBM SPSS® Statistics software version 29.0. The hypothesis test revealed that 2 out of 11 concentration sets of the binary mixture of AVO and BPO exhibited significant differences, specifically at BPO concentrations of 10 % and 60 %. Random errors diminish the precision of study findings but do not bring bias into the results, while systematic errors skew the research outcomes [27]. In this case, the result may be attributed to random error introduced during sample preparation, such as inconsistencies in syringe-based mixing or temperature fluctuations during FTIR analysis. The AVO and BPO samples were combined utilizing a 2 mL syringe to yield a final combination volume of 2 mL. The researcher's precision in reading the syringe scale may fluctuate during the mixing procedure, potentially resulting in random errors. Moreover, the adhesive properties of the oil adhering to the syringe surface may lead to residual sample retention, hence introducing unforeseen inaccuracies in the oil mixing procedure. External influences, such as variations in temperature and humidity during FTIR testing, can also influence the results, despite the routine acquisition of background spectra prior to sampling spectra.

The calibration and validation of result parameters from the binary mixture of AVO with LPO are presented in Table 5. The most efficient modeling to quantify LPO in the AVO binary mixture employed the PCR technique utilizing long wavenumbers of 1466–891 cm^{-1}. The modeling results indicated exceptionally low RMSEC and RMSEP values of 0.60 and 0.61, respectively. The R^2-cal and R^2-val values, both approximately 0.9998, showed that this model possesses a remarkably high predictive capability and can account for nearly all variability within the dataset. Furthermore, the RMSEP/RMSEC value of 1.01, which is nearly equal to 1, suggests a minimal danger of overfitting. The outcomes of the validation model predictions are nearly equal to those of the calibration model. Consequently, this model is considered accurate in estimating LPO in a binary mixture with AVO. Although PCR-based models, particularly those employing first derivative spectra, provided the most consistent results for both BPO and LPO adulteration, comparable performance was also observed with other approaches. Specifically, for the AVO/LPO mixture, both the PLS model using MSC-preprocessed original spectra and the SMLR model without preprocessing and without spectral derivatization yielded predictive accuracy within acceptable limits. These findings, as summarized in Table 5, underscore that no single chemometric method or spectral range can be universally recommended for all adulteration scenarios. Instead, method selection should consider both the nature of the adulterant and the intended analytical trade-offs between simplicity, accuracy, and robustness. Therefore, researchers are encouraged to examine a broad range of multivariate modeling approaches and spectral treatment techniques to identify the most suitable strategy for accurate quantification of adulterants across diverse sample

Table 5
The Efficacy of Multivariate Calibrations and Statistical Parameters in Estimating the Concentration of Branded Palm Oil and Loose Palm Oil as an Adulterant in Avocado Oil.

Multivariate	Pre-processing	Data Format	Branded Palm Oil							Loose Palm Oil						
			Recommended regions (cm^{-1})	RMSEC*	RMSEP*	RMSEP/ RMSEC*	R^2-cal	R^2-val	Factor/ PC	Recommended regions (cm^{-1})	RMSEC*	RMSEP*	RMSEP/ RMSEC*	R^2-cal	R^2-val	Factor/ PC
Classical Least Squares	None	Normal	1.664–894 (baseline)	1.51	0.810	0.54	0.9989	0.9997	-	3.470–895 (linear)	1.38	1.19	0.86	0.9990	0.9994	-
		First Derivative	1.737–890 (linear)	2.53	2.50	0.99	0.9968	0.9969	-	1.730–901 (linear)	1.38	1.10	0.80	0.9991	0.9994	-
		Second Derivative	1.734–1.694 (linear)	1.78	2.04	1.15	0.9984	0.9980	-	1.734–1.693 (linear)	2.04	2.18	1.07	0.9979	0.9980	-
Stepwise Multiple Linear Regression	None	Normal	-	1.33	1.20	0.90	0.9991	0.9993	-	-	0.96	0.99	1.02	0.9995	0.9995	-
		First Derivative	-	2.53	2.62		0.9969	0.9979	-	-	2.22	2.53	1.14	0.9975	0.9969	-
		Second Derivative	-	4.75	5.02	1.06	0.9887	0.9875	-	-	4.21	4.17	0.99	0.9920	0.9922	-
	MSC	Normal	-	0.87	0.77		0.9996	0.9998	-	-	1.26	1.45	1.15	0.9992	0.9992	-
		First Derivative	-	1.15	1.85	1.61	0.9993	0.9984	-	-	1.01	1.48	1.47	0.9995	0.9990	-
		Second Derivative	-	1.76	2.31	1.31	0.9985	0.9977	-	-	1.54	1.59	1.03	0.9988	0.9990	-
Partial Least Squares Regression	None	Normal	1.200–905 (none)	1.43	1.02	0.71	0.9990	0.9995	2	1.247–905 (none)	0.87	0.77	0.88	0.9996	0.9997	3
		First Derivative	1.163–890 (none)	0.12	0.86	7.16	1.0000	0.9996	6	1.466–891 (none)	0.61	0.68	1.11	0.9998	0.9998	3
		Second Derivative	1.734–1.125 (none)	0.31	1.35	4.35	1.0000	0.9991	7	1.740–1.125 (none)	0.34	1.47	4.31	0.9999	0.9992	6
	MSC	Normal	1.750–894 (none)	0.95	1.33	1.40	0.9995	0.9991	3	1.247–895 (none)	0.93	0.88	0.94	0.9996	0.9997	3
		First Derivative	1.735–901 (none)	0.25	0.53	2.12	1.0000	0.9999	6	1.749–902 (none)	0.84	1.00	1.19	0.9996	0.9996	3
		Second Derivative	1.734–1.702 (none)	1.16	1.09	0.94	0.9993	0.9994	4	2.868–1.732 (none)	0.39	1.37	3.48	0.9999	0.9993	3
Principal Component Regression	None	Normal	1.200–905 (none)	1.35	0.88	0.65	0.9991	0.9996	4	1.247–905 (none)	0.92	0.78	0.85	0.9996	0.9997	3
		First Derivative	1.163–890 (none)	0.95	0.89	0.94	0.9995	0.9996	10	1.466–891 (none)	0.60	0.61	1.01	0.9998	0.9998	10
		Second Derivative	1.734–1.125 (none)	0.74	1.57	2.12	0.9997	0.9988	10	1.740–1.125 (none)	0.95	1.77	1.87	0.9996	0.9989	10
	MSC	Normal	1.750–894 (none)	0.59	0.74	1.25	0.9998	0.9997	9	1.247–895 (none)	0.922	1.07	1.16	0.9996	0.9995	4
		First Derivative	1.735–901 (none)	0.56	0.55	0.98	0.9998	0.9999	10	1.749–902 (none)	0.77	0.91	1.18	0.9997	0.9997	10
		Second Derivative	1.734–1.702 (none)	1.11	0.89	0.80	0.9994	0.9996	10	2.868–1.732 (none)	1.10	1.45	1.32	0.9994	0.9992	10

MSC = Multiplicative Scatter Correction, R^2-cal = Calibration Model's Coefficient of Determination, R^2-val = Validation Model's Coefficient of Determination, RMSEC = Root Mean Square Error of Calibration, RMSEP = Root Mean Square Error of Prediction, Green highlight indicates the best quantification model, * = Rounded to two decimal places.

Table 6
Summary of Hypothesis Testing Between Actual and Predicted Data of Brand and Loose Palm Oils.

Actual - Avocado Oil (%)	Actual - Adulterant (%)	Calculated-Branded Palm Oil							Calculated-Loose Palm Oil						
		Calibration 1 (%)	Calibration 2 (%)	Calibration 3 (%)	Validation 1 (%)	Validation 2 (%)	Shapiro-Wilk Normality	Hypothesis Test * (p-value)	Calibration 1 (%)	Calibration 2 (%)	Calibration 3 (%)	Validation 1 (%)	Validation 2 (%)	Shapiro-Wilk Normality	Hypothesis Test * (p-value)
100	0	−0.37	−1.04	0.46	−0.31	−0.71	0.595	0.191	0.42	−0.41	0.29	0.42	0.48	0.012**	0.136
90	10	10.6	10.72	9.99	10.6	11.15	0.730	0.030***	8.91	10.18	10.07	10.28	10.76	0.287	0.902
80	20	19.17	19.83	19.36	20.75	20.01	0.564	0.560	20.08	20.48	20.26	20.52	20.90	0.867	0.032***
70	30	30.4	31.2	30.85	29.87	29.78	0.297	0.201	29.64	30.31	28.78	30.21	29.60	0.458	0.345
60	40	39.56	41.09	39.43	39.1	39.91	0.693	0.624	39.85	39.97	39.75	39.56	39.39	0.886	0.046***
50	50	49.73	50.11	49.49	49.35	49.6	0.513	0.057	51.23	51.17	50.68	51.07	50.79	0.407	<0.001***
40	60	59.87	59.94	59.25	59.02	59.41	0.238	0.048***	60.15	60.54	59.98	60.45	60.06	0.400	0.099
30	70	69.82	70.48	69.91	70.29	69.92	0.282	0.547	69.76	69.47	69.41	69.66	69.38	0.353	0.003***
20	80	80.4	79.98	79.92	79.19	79.98	0.014**	0.343	79.75	80.00	79.28	79.93	79.33	0.242	0.085
10	90	89.12	90.44	90.42	90.09	90.43	0.330	0.714	89.69	89.32	89.71	89.31	89.35	0.029**	0.043***
0	100	99.9	100.36	99.58	100.23	100.25	0.762	0.678	100.95	99.25	101.09	100.04	101.20	0.204	0.249

* = Test performed using one-sample *t*-test statistics if the sample is normally distributed and the Wilcoxon signed-rank test if the sample is not normally distributed, ** = Sample not normally distributed so that the Wilcoxon signed-rank test is used, *** = Actual sample and calculation are significantly different.

types.

Results of calculations derived from the best modeling were investigated with hypothesis testing. The summary of the normality test and hypothesis test is presented in Table 6, revealing that 5 out of the 11 concentration sets of the binary combination exhibited significant changes, specifically at LPO concentrations of 20 %, 40 %, 50 %, 70 %, and 90 %. Despite the model's satisfactory performance based on regression parameters for calibration and validation, the results are influenced by bias, potentially arising from persistent inaccuracies in the sample mixing procedure for binary mixes. The facile adhesion of AVO and LPO to the syringe surface heightens the probability of residual samples remaining on the syringe wall. This may lead to an imbalance in the composition of the resultant binary mixture, hence leading to the emergence of errors in the research process. Consequently, further study must be undertaken to validate the impact of the mixing process on the emergence of errors.

Bland–Altman plots, generated using Excel 2019, were employed to evaluate the concordance between predicted and observed concentrations of BPO and LPO. For BPO, the mean prediction difference was –0.04 (Fig. 5A), with data points symmetrically distributed around the zero-bias line and predominantly within the 95 % limits of agreement (±1.96 SD). This consistent dispersion suggests that the prediction errors of the model arise from inherent random variability rather than systematic bias. A comparable trend was noted for LPO, exhibiting a minimal mean difference of 0.05 and a random, balanced distribution of data points (Fig. 5B). Collectively, these findings substantiate the model's predictive accuracy and absence of systematic deviation across the concentration ranges.

For categorizing samples based on pure AVO or AVO adulterated with BPO, PCA-based discriminant analysis was conducted using TQ

Fig. 5. Bland–Altman Plot of BPO [A] and LPO [B] Predictions versus Actual Concentrations.

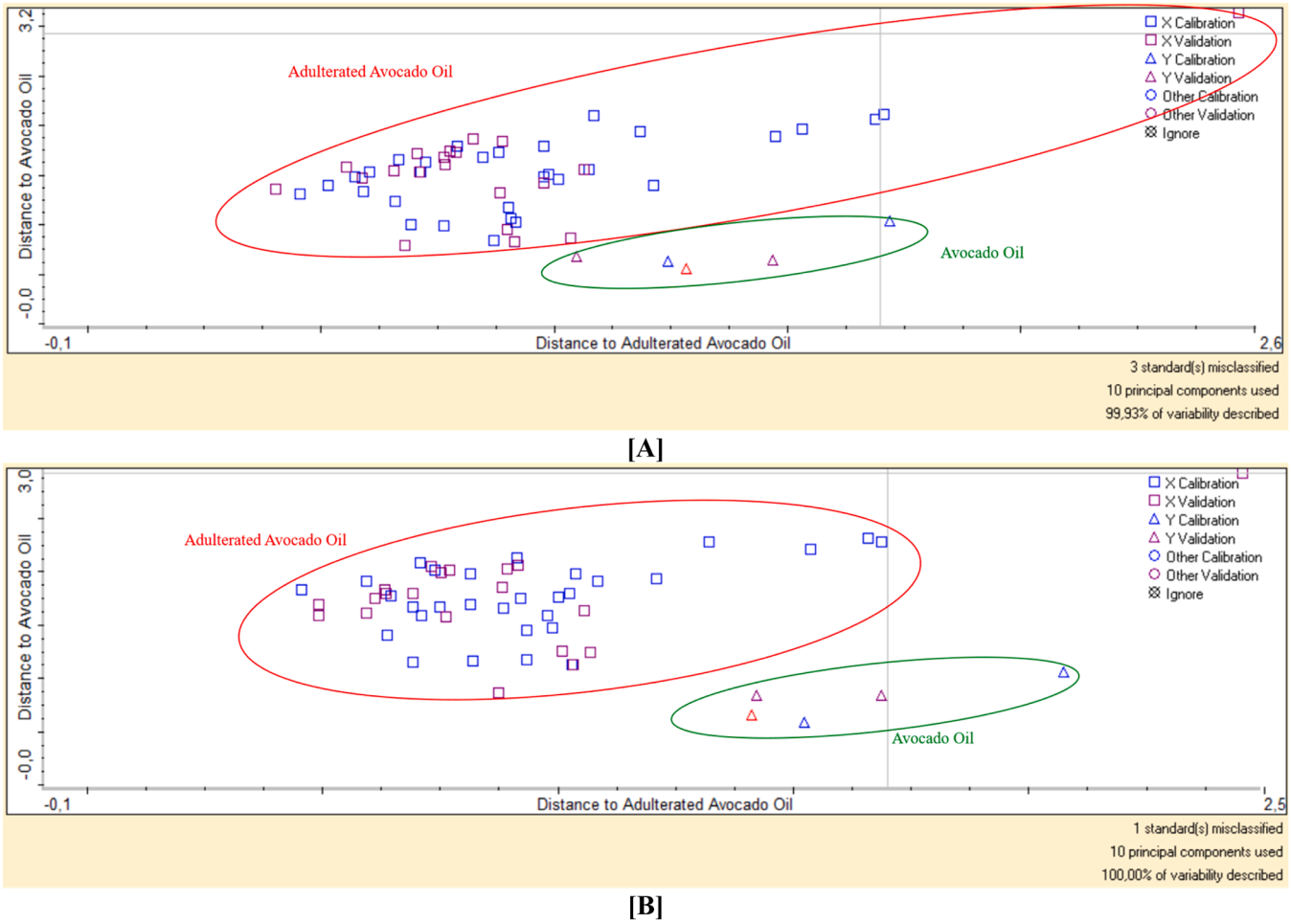


Fig. 6. Discriminant Analysis of Pure AVO with AVO Mixed with BPO using wavenumbers Recommendations 3932–668 cm $^{-1}$ [A] and 3055–2793 cm $^{-1}$ [B].

Analyst™ software version 9. The spectral data within the long wave range of 3932–668 cm^{-1}, as advised by the device software, enables the model to classify samples with an accuracy of 94.54 % (52 out of 55 sample readings) and accounts for 99.93 % of the data variability (Fig. 6A). Furthermore, the spectral data within the long wave range of 3055–2793 cm^{-1} demonstrate superior grouping capability, achieving an accuracy level of 98.18 % (54 out of 55 sample readings) and accounting for 100 % of the data variability (Fig. 6B). This evidence indicates that the integration of FTIR analysis with discriminant PCA was useful in grouping samples based on pure AVO or AVO mixed with BPO.

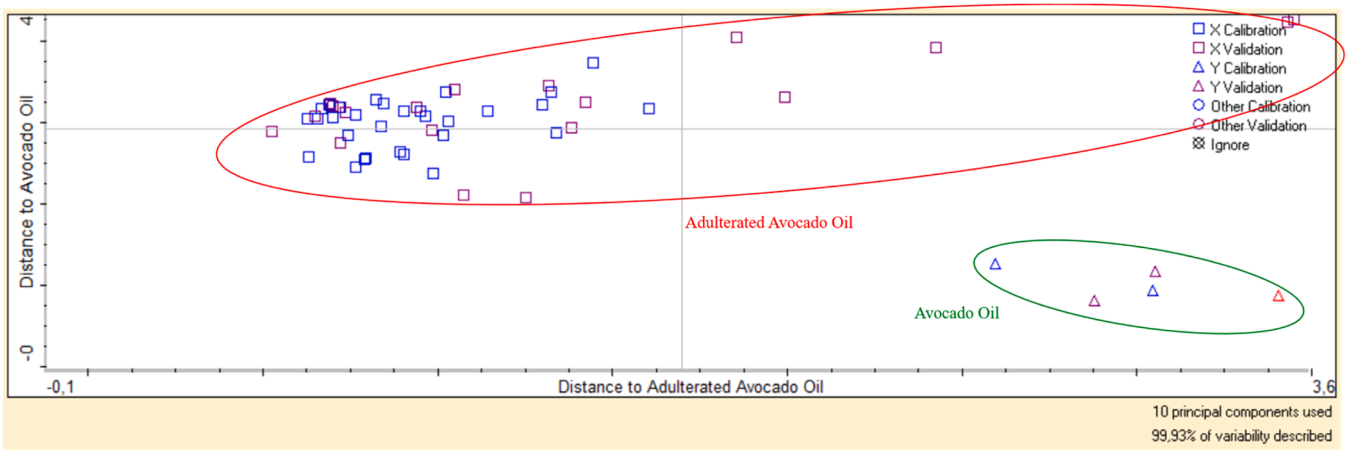
Classification of samples based on pure AVO and AVO combined with LPO conducted using PCA-based discriminant analysis. Spectral data within the wavenumber range of 3932–668 cm^{-1}, as advised by the device software, enables the model to categorize all samples with complete correctness, specifically 55 out of 55 sample readings (Fig. 7A). Furthermore, the spectral range of long waves from 3044 to 2771 cm^{-1} demonstrates effective clustering, achieving an accuracy of 100 % (55 out of 55 sample readings) and accounting for 99.99 % of data variation (Fig. 7B). These results indicate that the combination of FTIR analysis with PCA-based discriminant analysis is effective in differentiating samples, whether for pure AVO or AVO samples that have been adulterated with LPO.

Conclusions

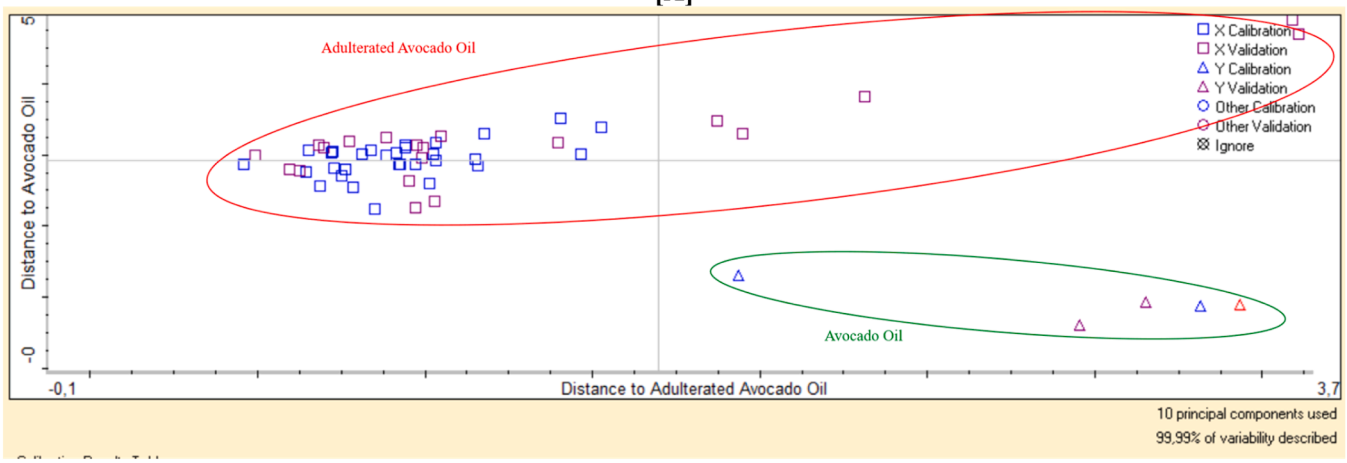
AVO can be distinctly categorized apart from BPO and LPO using FTIR analysis corroborated by PCA. PC1 is primarily influenced by absorption at a wavenumber of 1743 cm^{-1}, whereas PC2 is impacted by absorption at a wavenumber of 2953 cm^{-1}. PCR chemometrics with first derivative data and MSC correction correctly predicted the amount of BPO in AVO. This approach produces RMSEC and RMSEP values of 0.56 and 0.55, respectively, alongside R^2-cal and R^2-val values of 0.9998 and 0.9999, respectively. On the other hand, PCR chemometrics using first-derived data without MSC adjustment correctly predicted the levels of LPO in AVO, with RMSEC and RMSEP values of 0.60 and 0.61, respectively, along with R^2-cal and R^2-val values of 0.9998. With a correct classification rate of 98.18 % for BPO and 100 % for LPO, the PCA-based discriminant analysis correctly separated the real AVO samples from the adulterated AVO samples.

CRediT authorship contribution statement

David Fernando: Writing – original draft, Software, Project administration, Methodology, Formal analysis, Data curation, Conceptualization. **Desy Ayu Irma Permatasari:** Writing – original draft, Software, Methodology, Investigation, Formal analysis, Data curation.



[A]



[B]

Fig. 7. Discriminant Analysis of Pure AVO with AVO adulterated with LPO using Wavenumbers Recommendations 3932–668 cm $^{-1}$ [A] and 3044–2771 cm $^{-1}$ [B].

Agustina Ari Murti Budi Hastuti: Writing – original draft, Supervision, Software, Methodology, Formal analysis, Data curation, Conceptualization. **Abdul Rohman:** Writing – review & editing, Supervision, Software, Resources, Project administration, Methodology, Investigation, Formal analysis.

Declaration of competing interest

The authors declare that they have no known competing financial interests or personal relationships that could have appeared to influence the work reported in this paper.

Acknowledgements

We express our gratitude to the Indonesian Ministry of Education, Culture, Research, and Technology (Kemendikbudristek) for the financial support of this manuscript through the PMDSU (Pendidikan Magister menuju Doktor untuk Sarjana Unggul) program, as per decree number 0459/E5/PG.02.00/2024 and agreements/contracts number 048/E5/PG.02.00.PL/2024 and 2789/UN1/DITLIT/PT.

References

[1] A.M. Pérez-Calabuig, S. Pradana-López, A. Ramayo-Muñoz, J.C. Cancilla, J. S. Torrecilla, Deep quantification of a refined adulterant blended into pure avocado oil, Food Chem. 404 (2023) 134474, https://doi.org/10.1016/j.foodchem.2022.134474.

[2] H.S. Green, S.C. Wang, Purity and quality of private labelled avocado oil, in: Food Control, 152, Elsevier Ltd, 2023, https://doi.org/10.1016/j.foodcont.2023.109837.

[3] A. Woolf, M. Wong, L. Eyres, T. McGhie, C. Lund, S. Olsson, Y. Wang, C. Bulley, M. Wang, E. Friel, C. Requejo-Jackman, Avocado oil. Gourmet and health-promoting specialty oils, Elsevier, 2009, pp. 73–125, https://doi.org/10.1016/B978-1-893997-97-4.50008-5.

[4] H. Tapiero, D.M. Townsend, K.D. Tew, Phytosterols in the prevention of human pathologies, Biomed. Pharmacother. 57 (8) (2003) 321–325, https://doi.org/10.1016/S0753-3322(03)00104-5.

[5] X. Lin, Z. Li, Key components and multiple health functions of avocado oil: a review, J. Funct. Foods 122 (2024) 106494, https://doi.org/10.1016/j.jff.2024.106494.

[6] B. Cervantes-Paz, E.M. Yahia, Avocado oil: production and market demand, bioactive components, implications in health, and tendencies and potential uses, in: Compr. Rev. Food Sci. Food Saf., 20, Blackwell Publishing Inc, 2021, pp. 4120–4158, https://doi.org/10.1111/1541-4337.12784.

[7] International Monetary Fund, Primary Commod. Price Syst (2023). https://legacydata.imf.org/?sk=471dddf8-d8a7-499a-81ba-5b332c01f8b9.

[8] D. Fernando, P. Marbun, A.A.M.B. Hastuti, A. Rohman, Current trends and future directions in avocado oil research: an overview and a bibliometric analysis across two time points, Oil Crop. Sci. 10 (1) (2025) 25–43, https://doi.org/10.1016/j.ocsci.2025.02.003.

[9] France Eurofins Analytics, J.-F. Morin, M. Lees, FoodIntegrity Handbook: A Guide to Food Authenticity Issues and Analytical Solutions, Eurofins Analytics France, 2018, https://doi.org/10.32741/fihb, 1st ed.

[10] H. Swartz, The ethics of labeling food safety risks, Food Ethics 2 (2–3) (2019) 127–137, https://doi.org/10.1007/s41055-019-00035-7.

[11] P. Visciano, M. Schirone, Food Frauds: global incidents and misleading situations, Trends Food Sci. Technol. 114 (2021) 424–442, https://doi.org/10.1016/j.tifs.2021.06.010.

[12] K. Everstine, B. Popping, S.M. Gendel, Food fraud mitigation: strategic approaches and tools. Food Fraud, Elsevier, 2021, pp. 23–43, https://doi.org/10.1016/B978-0-12-817242-1.00015-4.

[13] D.I. Ellis, V.L. Brewster, W.B. Dunn, J.W. Allwood, A.P. Golovanov, R. Goodacre, Fingerprint. Food: Current Technologies for the Detection of Food, Chem. Soc. Rev. (2012).
[14] K. Candoğan, E.G. Altuntas, N. İğci, Authentication and quality assessment of meat products by fourier-transform infrared (FTIR) spectroscopy, Food Eng. Rev. 13 (1) (2021) 66–91, https://doi.org/10.1007/s12393-020-09251-y.
[15] R. Saji, A. Ramani, K. Gandhi, R. Seth, R. Sharma, Application of FTIR spectroscopy in dairy products: a systematic review, Food Humanity 2 (2024) 100239, https://doi.org/10.1016/j.foohum.2024.100239.
[16] A. Rohman, F.A. Lumakso, S. Riyanto, Use of partial least square-discriminant analysis combined with mid infrared spectroscopy for avocado oil authentication, Res. J. Med. Plant. 10 (2) (2016) 175–180, https://doi.org/10.3923/rjmp.2016.175.180.
[17] N. Quiñones-Islas, O.G. Meza-Márquez, G. Osorio-Revilla, T. Gallardo-Velazquez, Detection of adulterants in avocado oil by mid-FTIR spectroscopy and multivariate analysis, Food Res. Int. 51 (1) (2013) 148–154, https://doi.org/10.1016/j.foodres.2012.11.037.
[18] P. Jiménez-Sotelo, M. Hernández-Martínez, G. Osorio-Revilla, O.G. Meza-Márquez, F. García-Ochoa, T. Gallardo-Velázquez, Use of ATR-FTIR spectroscopy coupled with chemometrics for the authentication of avocado oil in ternary mixtures with sunflower and soybean oils, Food Addit. Contam. - Chem. Anal. Control Expo. Risk 33 (7) (2016) 1105–1115, https://doi.org/10.1080/19440049.2016.1203073.
[19] I. Santana, L.M.F. Dos Reis, A.G. Torres, L.M.C. Cabral, S.P. Freitas, Avocado (Persea americana Mill.) oil produced by microwave drying and expeller pressing exhibits low acidity and high oxidative stability, Europe. J. Lipid Sci. Technol. 117 (7) (2015) 999–1007, https://doi.org/10.1002/ejlt.201400172.
[20] C. Nasri, Y. Halabi, H. Harhar, F. Mohammed, A. Bellaouchou, A. Guenbour, M. Tabyaoui, Chemical characterization of oil from four avocado varieties cultivated in Morocco, OCL 28 (2021) 19, https://doi.org/10.1051/ocl/2021008.
[21] D. Fernando, D. Santosa, A. Rohman, Using macroscopic, microscopic, and FTIR spectroscopy combined with chemometrics to authenticate arabica coffee from Antbush, Maj. Obat Tradis. 29 (1) (2024) 69, https://doi.org/10.22146/mot.85039.
[22] H. Zhan, J. Fang, L. Tang, H. Yang, H. Li, Z. Wang, B. Yang, H. Wu, M. Fu, Application of near-infrared spectroscopy for the rapid quality assessment of Radix paeoniae Rubra, Spectrochim. Acta - A: Mol. Biomol. Spectrosc. 183 (2017) 75–83, https://doi.org/10.1016/j.saa.2017.04.034.
[23] M.J. Lerma-García, G. Ramis-Ramos, J.M. Herrero-Martínez, E.F. Simó-Alfonso, Authentication of extra virgin olive oils by fourier-transform infrared spectroscopy, Food Chem. 118 (1) (2010) 78–83, https://doi.org/10.1016/j.foodchem.2009.04.092.
[24] F.A. Lumakso, A. Rohman, M. Handoy, S. Riyanto, F.Mohd Yusuf, Detection and quantification of soybean and corn oils as adulterants in avocado oil using fourier transform mid infrared (FT-MIR) spectroscopy aided with multivariate calibration, in: J. Teknol., 77, Penerbit UTM Press, 2015, pp. 251–255, https://doi.org/10.11113/jt.v77.3640.
[25] J. Coates, Interpretation of infrared spectra, A practical approach, Ed., in: R. A. Meyers (Ed.), Encyclopedia of Analytical Chemistry, John Wiley & Sons, Ltd, 2006, p. a5606, https://doi.org/10.1002/9780470027318.a5606.
[26] D.L. Pavia, G.M. Lampman, G.S. Kriz, Introduction to spectroscopy, Saunders College Division, 2001, 3rd ed.
[27] G.J. Mellenbergh, Random and systematic errors in context, Ed., in: G. J. Mellenbergh (Ed.), Counteracting methodological errors in behavioral research, Springer International Publishing, 2019, pp. 1–12, https://doi.org/10.1007/978-3-030-12272-0_1.